Hydrogen bioelectrooxidation on gold nanoparticle-based electrodes modified by Aquifex aeolicus hydrogenase: Application to hydrogen/oxygen enzymatic biofuel cells

Karen Monsalve, Magali Roger, Cristina Gutierrez-Sanchez, Marianne Ilbert, Serge Nitsche, Deborah Byrne-Kodjabachian, Valérie Marchi, Elisabeth. Lojou

Hydrogen bioelectrooxidation on gold nanoparticle-based electrodes modified by *Aquifex aeolicus* hydrogenase: application to hydrogen/oxygen enzymatic biofuel cells

Karen Monsalve[(a)], Magali Roger[(a)], Cristina Gutierrez-Sanchez[(a)], Marianne Ilbert[(a)], Serge Nitsche[(b)], Deborah Byrne-Kodjabachian[(c)], Valérie Marchi[(d)], Elisabeth Lojou[(a)]✉

[(a)] *Bioénergétique et Ingénierie des Protéines, UMR 7281, CNRS-AMU, 31 Chemin Aiguier, 13009 Marseille, France.*

[(b)] *CINaM, Campus de Luminy, Case 913, 13288 Marseille Cedex 9, France*

[(c)] *IMM CNRS-AMU, 31 chemin Joseph Aiguier, 13009 Marseille, France*

[(d)] *Université Rennes 1, Institut des Sciences Chimiques de Rennes, CNRS UMR 6226 Campus de Beaulieu, 35042 Rennes, France*

✉ Corresponding author: Tel : +33 491164524; fax : +33 491164097; e-mail address : lojou@imm.cnrs.fr

Abstract

For the first time, gold nanoparticle-based electrodes have been used as platforms for efficient immobilization of the [NiFe] hydrogenase from the hyperthermophilic bacterium *Aquifex aeolicus*. AuNPs were characterized by electronic microscopy, dynamic light scattering and UV-Vis spectroscopy. Two sizes around 20.0±5.3 nm and 37.2±4.3 nm nm were synthesized. After thiol-based functionalization, the AuNPs were proved to allow direct H_2 oxidation over a large range of temperatures. A high current density up to 1.85±0.15 mA.cm^{-2} was reached at the smallest AuNPs, which is 170 times higher than the one recorded at the bare gold electrode. The catalytic current was especially studied as a function of the AuNP size and amount, and procedure for deposition. A synergetic effect between the AuNP porous deposit and the increase surface area was shown. Compared to previously used nanomaterials such as carbon nanofibers, the covalent grafting of the enzyme on the thiol-modified gold nanoparticles was shown to enhance the stability of the hydrogenase. This bioanode was finally coupled to a biocathode where BOD from *Myrothecium verrucaria* was immobilized on AuNP-based film. The performance of the so-mounted H_2/O_2 biofuel cell was evaluated, and a power density of 0.25 mW.cm^{-2} was recorded.

Keywords: Gold nanoparticles; Hydrogenase; Bilirubin oxidase; Direct electron transfer, Enzymatic H_2/O_2 biofuel cell.

1. Introduction

Enzymatic biofuel cells (EBFCs) have emerged as sustainable biodevices alternative to low temperature proton membrane exchange fuel cells for small portable electrical alimentation [1-3]. A new generation of EBFCs has been developed very recently based on [NiFe] hydrogenases and multicopper oxidases such as bilirubin oxidases as efficient biocatalysts for H_2 oxidation and O_2 reduction respectively [4]. Thanks to the use of inhibitor-tolerant and thermostable enzymes immobilized on 3D-carbon networks, power densities in the range of the mW/cm^2 were reached at neutral pH over a large range of temperatures [5-8]. Some limitations were however highlighted which need to be overcome before EBFCs can be used in commercial devices. Especially, mass transfer processes require design and modeling of the porous electrodes, and stability of the biohybrids is to be circumvented. One more key requirement to improve enzyme connection, then to yield higher current densities, is the accurate knowledge of the electrically connected enzymes at the electrochemical interface. This will also provide the fundamental missing data which are necessary to understand than remediate the instability of the electrocatalytic signal.

In the search for efficient electron transfer between enzymes and electrified interfaces, nanoparticles have attracted increasing interest. Due to quantum size effect, nanoparticles display physical properties that are different from bulk metal [9]. It is particularly important when they are used in electrochemistry because they exhibit size-dependent surface adsorption properties and charge donation/acceptance capabilities which determine the electrocatalytic pathways and kinetics [10]. Long distance electron transfer can be affected in case of very small size nanoparticles which approach the effective electron tunneling distances (< 5 nm). In bioelectrochemistry, AuNP variable size and electronic properties are expected to provide versatile building blocks as well as large surface area-to-volume ratios suitable for high enzyme loading. The activity, stability and electron transfer properties may be altered at nanostructured interfaces compared to flat surfaces, especially when the curvature of the nanoparticle is comparable to the size of the enzyme [11-13]. Because gold nanoparticles (AuNPs) with controlled sizes can be quite easily prepared and functionalized by versatile thiol chemistry, AuNP films on electrochemical interfaces have been targeted. It was demonstrated that AuNPs can act as conductive wires between the enzymes and the electrode. Long range electron transfer and efficient catalysis were highlighted for various proteins and enzymes immobilized on AuNP films, such as heme proteins including membrane cytochrome oxidases [14-17], azurin, a blue copper protein [18], glucose oxidase [19, 20], and sulfite oxidase [21]. Porous 3D-networks of AuNPs obtained by drop casting of concentrated gold colloids were shown to enhance electrocatalysis by bilirubin oxidase (BOD) [22, 23], cellobiose dehydrogenase [24], and laccase [25-28]. Sugar/O_2 BFCs were accordingly constructed with AuNP-based bioanode and biocathode [29-31].

Aquifex aeolicus [NiFe] membrane bound hydrogenase (*Aa* MbH1) is one of the identified hydrogenases which present O_2-, CO- and temperature tolerances [32-34]. Direct electrical connection of this enzyme was already shown on graphite, carbon nanotubes, carbon nanoparticles and carbon nanofibers (CNFs) [35-37]. Thiol modified gold electrodes were also studied as platforms for hydrogenases [38-39]. Electron transfer proceeds from the [NiFe] active site buried inside the large subunit to the surface of the enzyme *via* a conductive line of three FeS clusters. Combining electrochemistry, Atomic Force Microscopy, Polarization Modulation Infrared Reflection Adsorption Spectroscopy (PMIRRAS) and molecular dynamics at self-assembled-monolayers on gold, it was demonstrated that the transmembrane helix close to the surface FeS electron relay and surrounded by detergent controlled the immobilization of the enzyme [38, 40]. Decrease of the catalytic current with

time was however often observed. But because the amount of enzyme effectively participating to the current is unknown, the reasons for such a decrease are difficult to establish. Release but also change in orientation or in structural conformation of the enzyme upon time, applied potential or environmental conditions may account for the signal evolution. One elegant way would be to couple electrochemistry to other methods such as Quartz Crystal Microbalance (QCM), Surface Plasmon Resonance (SPR) and surface spectroscopies (SEIRA, SERRS or PMIRRAS for example), which most often rely on gold substrates. In this context, it would be of high interest to increase the signal/noise ratio by enzyme immobilization on NPs. We report here the first step toward this objective. The direct electrocatalytic oxidation of hydrogen by *Aa* MbH1 immobilized on AuNP deposited on gold electrodes is demonstrated for the first time. The influence of AuNP film structure on both the amount of electrically connected enzymes and the electron transfer rate is studied. The bioanode is coupled to a biocathode based on BOD from *Myrothecium verrucaria* (*Mv* BOD) also immobilized on AuNP-based film, and the performance of the so-mounted H_2/O_2 EBFC is evaluated. Promising results are obtained which compare well to the previous H_2/O_2 EBFC based on carbon nanomaterials.

2. Experimental

2.1. Chemicals and materials

All solutions were prepared with Milli-Q water (18.2 MΩ·cm). Biphenyl-4,4'-dithiol (BPDT), 3-mercaptopropionic acid (3-MPA), 6-mercaptohexanoic acid (6-MHA), 4-aminothiophenol (4-ATP) for gold electrode or AuNP functionalization were prepared to a final concentration of 5 mM in 90/10 v/v ethanol/water solutions. 2,2'-azino-bis(3-ethylbenzothiazoline-6-sulphonic acid) (ABTS) was used as a substrate for bilirubin oxidase activity. 50 mM 4-(2-hydroxyethyl)piperazine-1-ethanesulfonic acid (HEPES) buffer pH 7.2, and 10 mM phosphate buffer pH 6 were used for hydrogenase solution deposited on pyrolytic graphite (PG) and gold electrodes respectively. Bilirubin oxidase solution was prepared in 10 mM phosphate buffer pH 7. Covalent grafting of the enzymes was realized with 14 mM 1-(3-dimethylamino-propyl)-3-ethylcarbodiimide (EDC) and 21 mM N-hydroxysuccinimide (NHS) in the presence of 10 mM morpholino-ethanesulphonic acid (MES) buffer pH 6. Gold (III) chloride solution 30 wt. % and sodium citrate were used for AuNP synthesis. CNF were synthesized as in [39] and prepared in solution (50:50) of Milli-Q water and dimethylformamide to a final concentration of 4 $mg.mL^{-1}$ and sonicated for 30 min. n-Dodecyl α-D-maltoside (DDM) with a critical micelle concentration (CMC) of 0.18 mM at 25°C was diluted in water. It was quantified using thin layer chromatography as described in Ciaccafava *et al.* [35]. All chemicals were purchased from Sigma-Aldrich. *Aa* MbH1 was purified as described in Luo *et al.* [32]. *Mv* BOD was a gift from Amano Enzyme Inc. (Nagoya, Japan). Purity of the enzymes was checked on 12% SDS-PAGE gel.

2.2. Instrumentation and measurement procedures

Electrochemical experiments were performed using a potentiostat from Autolab with Nova software. The Ag/AgCl (NaCl sat.) reference electrode was separated from the electrolyte using a side junction maintained at room temperature. A polycrystalline gold electrode from Materials Mates was the working electrode (projected surface area A=0.0078 cm^2). Unless specified, all current densities reported in this paper were calculated using the real gold electroactive surface area obtained by integration of the gold oxide reduction peak at +0.9 V, taking into account a charge of 390 $\mu C.cm^{-2}$ for the reduction of a gold oxide monolayer [41] (the electroactive surface area of the gold electrodes are between 2 and 5

times higher than the projected geometric area according to the electrode). Measurements of the electroactive gold surface of the bare gold electrode (AuE) and of the gold nanoparticle modified gold electrode (AuNP/AuE) were done by cyclic voltammetry in 0.05 M H_2SO_4, under N_2 and room temperature. The gold electroactive surface increase due to nanoparticle casting was defined as the ratio between the surface developed by the gold nanoparticles and the bare gold surface. It is denoted AuNPs/AuE. For the biofuel cell measurement, the electrodes were placed at 6 cm from the Nafion® membrane (Nafion® 117 from DUPONT-USA) separating the compartments. The biofuel cell performances were examined with a constant supply of substrate of 100 % H_2 and 100 % O_2 for anode and cathode respectively. Gas bubbling at an optimized flow rate of 5 cm^3/s was maintained into the electrolyte solution to limit substrate depletion. Each half-cell was independently thermo-regulated. The cell current and voltage were measured by polarization curves, after stabilization of the system. Scan rate was 3 mV/s. All the experiments are at least three times replicated.

Transmission Electron Microscopy (TEM) was performed with the high transmission resolution electron microscope JEM 3010 (JEOL HRTEM). 1 µL of AuNP suspensions were deposited on 300 mesh copper grid carbon film and let dry. Scanning Electron Microscopy (SEM) was performed with the high scanning resolution microscope JSM 6320F (JEOL FEGSEM). Three successive castings of 1µL of AuNP dispersion were deposited on a flat gold support to mimick the gold deposit on the gold electrode and let dry. Average AuNP diameter and standard deviations were calculated from each sample using ImageJ software.

Dynamic Light Scattering (DLS) experiments were performed using a Zetazizer Nano Series (Malvern Instruments, London, UK). The AuNPs were analyzed in a disposable micro-cuvette ZEN0040 after 2 min equilibration within the instrument at 25°C. All measurement conditions were optimized automatically by the instrument software. The results are reported as the average of 3 measurements consisting of 11 runs each with a run duration of 10 seconds. The size determination in polydisperse samples was determined by the distribution analysis based on Multiple Narrow Modes non-negative least squares analysis in high resolution with 300 classes to give a more detailed spectrum.

UV-visible experiments were recorded using a Cary-Win UV-visible spectrophotometer.

2.3. Nanoparticle synthesis

AuNP synthesis was performed by citrate reduction of $HAuCl_4$ in water as previously described [42]. Briefly, 12.5 mL of 38.8 mM sodium citrate were added to 125 mL of boiling 1mM $HAuCl_4$ solution under vigorous stirring leading to nanoparticle formation. After 15 min of reaction, the reactants were let to cool down at room temperature. The deep red color of AuNPs in water reflects the Surface Plasmon Band (SPB), a broad absorption band in the visible region around 520 nm, whose intensity decreases and position increases with the size of the NP [43, 44]. AuNP size was followed by UV spectrophotometry and additionally confirmed by DLS and TEM. To increase the number of AuNPs per volume, the AuNP solution was centrifuged (15 min, 10 000*g*) in 1.5 mL Eppendorf tubes; then 98% of the remaining supernatant volume was thrown away. The precipitant was suspended by ultrasonication and stored at 4°C. To prepare larger nanoparticles, less amount of the sodium citrate reducing agent (19 mM) was used while keeping the same auric chloride concentration.

2.4. Electrode preparation

Gold electrode surface (AuE) was cleaned by immersion in Regia water (3:1 concentrated HCl:HNO_3), rinsed with Milli-Q water and then polished successively with 1, 0.3 and 0.04 µm alumina slurry (ESCIL, Lyon, France) on a cloth polishing pad (PRESI).

During the polishing step intervals the electrodes were rinsed with Milli-Q water, then electrodes were dipped in a Milli-Q ultrasonic water bath for few seconds. Finally, electrochemical cleaning was done by cycling in 0.05 M H_2SO_4 solution between -0.35 V and +1.5 V at 0.1 V/s until reproducible voltammograms were obtained. To obtain nanostructured AuNP/AuE electrodes, 1µL of concentrated AuNPs was cast on the surface of a previously cleaned AuE and evaporated. This procedure was repeated consecutively. To determine the increase in the electroactive gold surface cyclic voltammetry measurements were performed in 0.05 M H_2SO_4 solution between -0.35V and +1.5V at a scan rate of 0.1 V/s under N_2 atmosphere until stable voltammograms were obtained (around 30 cycles). The AuE or AuNP/AuE electrodes were then immersed in 5 mM thiolated compound solutions for 12 hours for chemical functionalization. The thiol-modified electrodes were thoroughly rinsed with ethanol then with Milli-Q water to remove physically absorbed thiols.

Aa MbH1 and *Mv* BOD were either physically adsorbed to the thiol layer or covalently bound with 5.5µL of 14 mM EDC and 4.5 µL of 21 mM NHS. The mixture was left for 90 min at 4°C, then the enzyme-modified electrodes were rinsed with Milli-Q water to remove non covalently attached enzymes.

CNF/PG electrodes were prepared by three successive deposits of 5µL CNF solution. Between each layer the deposit was dried at 60°C for 5 min. Current densities for the CNF/PG electrodes were calculated using the geometric area of the PG electrode (0.0706 cm^2).

Electrochemical experiments were carried out in 10 mM phosphate buffer, pH 6 and 50 mM HEPES buffer, pH 7.2 for Au-based electrodes and PG-based electrodes respectively.

3. Results and Discussion

3.1. Characterization of AuNP deposit on gold electrodes

The morphology and size distribution of the AuNPs were evaluated by DLS, HRTEM and UV-visible spectroscopy (Figure 1). DLS experiments showed that the AuNP preparation is stable over a 6 month storage period. According to the size distribution by mass, the AuNP preparation synthesized with 38.8 mM sodium citrate contains two populations around 27 nm and 140 nm (Figure 1A). 94 % of the population is 26.6±2 nm however. The surface plasmon band in UV-Visible spectra is obtained at 524 nm (Figure 1B), as expected for AuNPs with a size range around 25 nm [43]. TEM images of AuNP solutions reveal a non-strictly uniform size most probably due to some aggregation during solvent evaporation. The AuNPs are however well resolved with average diameter size of 20.0±5.3 nm (Figure 1C). As hydrodynamic diameters from DLS measurements represent the size of particles continuously moving in the solution and as it takes into account the citrate-coating corona around the particles, larger size dimensions are generally obtained than observed by microscopy where the samples are fixed and dried. The three methods are then in good agreement. For the nanoparticles synthesized with 19.4 mM sodium citrate, the plasmon band shifted towards 532 nm (Figure 1B). In accordance with this plasmon band shift, larger size nanoparticles are observed by TEM yielding AuNPs with average size of 37.2±4.3 nm (Figure 1D).

To modify the bare gold electrode (AuE), 1 µL of concentrated AuNPs was deposited, followed by evaporation. Increasing cycles of "casting-evaporation" were repeated, and the consecutive increases in the electroactive surface area were evaluated using cyclic voltammetry (CV). Typical CVs obtained by consecutive AuNP colloid drops on the AuE are shown in Figure 2A. The amount of charge under the gold oxide reducing peak at + 0.9 V *vs*. Ag/AgCl increases with increasing castings. From integration of this reduction peak, the real electroactive surface area is evaluated taking into account a theoretical charge of 390±10 $\mu C.cm^{-2}$ for the reduction of a gold oxide monolayer [41]. When reported to the real

electroactive surface of the unmodified AuE evaluated similarly than the modified electrode, a linear relationship is obtained at least for up to four drop casting layers (Figure 2B). This suggests that all the AuNPs participate to the electroactive surface. A value for AuNPs/AuE of more than 50 is reached after four drop castings. Similarly, Murata *et al*. showed that even with 15 drop castings of AuNPs almost all the AuNPs were interconnected [45].

The AuNPs/AuE developed surface was further analyzed using SEM (Figure 2C). A three dimensional nanostructured network develops in which well-defined spherically-shaped AuNPs separated by nanoholes are observed. The average size of the AuNPs is 22 ± 3.2 nm which agrees with the size previously determined. Both the preservation of size and morphology of the AuNPs and the porous nature of the deposit are expected to be of great interest for enzyme electrochemistry. Enzyme attachment will take benefit of the AuNP property, while the porosity will help mass transport of substrates.

3.2. Electroenzymatic oxidation of H_2 on AuNPs

CVs of direct H_2 oxidation by *Aa* MbH1 directly adsorbed on one casting of AuNPs on a gold electrode are shown in Figure 3. Because this hydrogenase is O_2-tolerant, a high current for H_2 oxidation can be obtained under H_2 atmosphere with the electrochemical cell directly on the bench. H_2 was first maintained in over pressure above the electrolyte (Figure 3, curve a). A plateau shape was recorded which is very much like the shape previously observed by modification of a graphite electrode by CNFs [37]. We demonstrated that this particular shape was related to mass transport limitation inside the mesoporous CNF film, and could be circumvented by bubbling H_2 inside the electrolyte. AuNP deposit generates the same limitation since recording the CV with continuous H_2 flow inside the electrolyte results in an increase in the catalytic current and the appearance of a classical CV shape for H_2 oxidation by adsorbed [NiFe] hydrogenase (Figure 3, curve b) [33]. This classic bell shape is characterized at pH 6 and 60°C by an onset potential of - 0.5 V *vs*. Ag/AgCl for H_2 oxidation in relation with the redox potentials of the FeS cluster, an increase in current as the catalysis proceeds, followed by a decrease of the current at potentials higher than - 0.2 V *vs*. Ag/AgCl related to the formation of an inactive state of the enzyme. This is a reversible process as H_2 is again oxidized on the reverse scan. No reduction of protons can be observed as expected for O_2-tolerant hydrogenases [33]. The addition of a redox mediator in solution (methylene blue is suitable for mediated oxidation using this typical hydrogenase [38]) resulted in a very small additional catalytic current. Most hydrogenase molecules are thus electrically connected to the AuNPs. As expected, no oxidative currents can be detected under N_2 or in the absence of hydrogenase (Figure 3, curve c and SI 1).

Previous studies dedicated to *Aa* MbH1 immobilization on thiol-based self-assembled-monolayer emphasized that efficient catalytic H_2 oxidation can be obtained either with amino- or carboxylic-end functions [38]. This behavior was rationalized by taking into account the low value of the dipole moment of the protein which furthermore presents a large variation in direction [40]. Similarly, immobilization of the hydrogenase on 4-ATP or 3-MPA modified AuNPs allows direct and efficient H_2 oxidation (data not shown). The affinity of the hydrogenase for both positively and negatively charged interfaces is thus preserved at the nanoparticles. In this work, 4-ATP was preferred over 3-MPA to functionalize the nanoparticles because of a higher stability over time under the reducing experimental conditions that are required for the catalytic H_2 oxidation by the hyperthermophilic hydrogenase. This is in agreement with the previous study dedicated to hydrogenases from *Desulfovibrio* on gold electrodes [46]. Compared to the signal obtained at the bare AuE, AuNP nanostructure induces a great enhancement of the catalytic current. The higher the AuNP developed surface, the higher the catalytic current (Figure 4A). Current density for H_2

oxidation reaches 1.85 ± 0.15 mA.cm^{-2} for AuNPs/AuE around 50, which is up to 170 times higher than at the bare AuE. Although the electroactive surface is greatly increased, and even for the highest AuNPs/AuE values, no non catalytic signals could be observed under N_2 atm.

Horse heart cytochrome c (cyt c) was also adsorbed on AuNP deposits modified by 6-MHA (Table 1 in SI). The AuNP modified gold electrode was incubated with 10 µL of 50 µM cytochrome c for 1 h at 4°C. A well defined redox wave developed at 0 V *vs*. Ag/AgCl characteristic of the Fe^{III}/Fe^{II} transition of the hemic center. The increase in the peak currents, either anodic or cathodic, was almost proportional to the increase in the surface area, hence denoting that it was mostly related to more proteins immobilized on a larger electroactive surface area. The same linear relation between the amount of cyt c and the number of deposits was mentioned by Murata *et al.* [22]. In contrast, the authors reported that O_2 reduction by bilirubin oxidase (BOD) rapidly reached a saturation value, suggesting that the difference in size between cyt c and BOD could control the immobilization process in the depths of the AuNP assembly. To have a better understanding of the behavior of hydrogenase, the catalytic current density was reported to the electroactive surface developed by the AuNPs (Figure 4B) calculated for each electrode by CV and peak integration as described above. Three domains can be clearly defined as a function of AuNPs/AuE. For the lowest AuNPs/AuE, between 1 and 10, the increase in the catalytic current is simply related to the increase in the surface area, as denoted by the constancy of the current densities reported to the electroactive area developed by the AuNPs. In this first domain, the current density reported to the surface developed by the AuNPs is in the order of 10 µA.cm^{-2}. This value is very close to the current density obtained at the bare AuE. This most probably reflects the first step of AuNP deposition on the electrode as a rather flat deposit. A second domain can be observed for higher AuNPs/AuE, i.e. between 10 and up to 25. An enhancement of the current density much above the enhancement of the surface is observed as highlighted in Figure 4B. In this domain, the current density reported to the AuNP developed surface area gradually increases up to 0.08 mA.cm^{-2}. A synergic effect between the increase in the electroactive surface and the morphology of the AuNP film may account for that phenomenon. This step involves most probably the formation of the microporous structure as shown in Figure 2C, which is favorable to a high amount of connected hydrogenase displaying a high electron transfer rate. The third domain concerns AuNPs/AuE between 25 and 50, where the current density reported to the surface developed by the AuNPs decreases then tends to stabilize as the value AuNPs/AuE increases. In this step, as the thickness increases, it can be hypothesized that the structure of the deposit becomes less porous, thus less adapted to a high efficiency of the enzyme.

When the hydrogenase is adsorbed on higher size AuNPs obtained by using a lower citrate concentration, the catalytic current is lower as already noticed for other enzymes such as cytochrome *bo3* oxidase [17] or laccase [25] (Figure SI 2). A lower increase in the surface area was also measured. AuNPs/AuE was experimentally always inferior to 6. The catalytic current reported to the surface area developed by the AuNPs is close to 10 µA.cm^{-2}, falling into the current density range obtained for the same AuNPs/AuE domain with the smaller size AuNPs. As shown in Figure SI 2 whatever the nanoparticle size, no shift in the catalytic potential can be observed. It thus appears that the size of the AuNP has little influence on the electron transfer rate. In a recent work, Shleev's group investigated the influence of NP size on the electron transfer rate for O_2 reduction by BOD [47]. The main conclusion was that the use of NPs with size higher than the enzyme dimension induced no influence on the electron rate. The same conclusion can be drawn from our experiments. One must suspect however that the formation of a microporous structure with suitable cavities for hydrogenase entrapment may help in the enhancement of the electrocatalysis once a certain thickness of

AuNPs is reached. Other methods than electrochemistry are now necessary to confirm this assumption.

The stability of the AuNP/*Aa* MbH1 biohybrid was first followed over one hour by chronoamperometry at a potential of -0.3 V *vs.* Ag/AgCl (Figure 5). During this short period, all the weakly attached materials, AuNPs and enzyme-AuNPs are expected to contribute to the current loss. It is observed that 50% of the initial catalytic current is lost after continuous working of the enzyme absorbed on the AuNP modified electrode at 60°C and under H_2 atmosphere (Figure 5A, curve a). If a covalent attachment is done between the hydrogenase and the amino group of the 4-ATP layer *via* EDC/NHS coupling there is an improvement of the stability of the bioelectrode. The current decrease is only 25% (Figure 5A, curve b). Because *Aa* MbH1 is a membrane bound hydrogenase, it is extracted from the cell membrane using the neutral detergent DDM. We previously demonstrated that the amount of detergent was crucial for enzyme stability, while a high amount of detergent might affect the electrochemical signal [39]. In this work, an optimized amount of DDM in the enzyme solution was found to be close to 3 times the CMC (i.e. 0.54 mM). In these conditions, the current loss is only 11 % after one hour of continuous catalysis (Figure 5A, curve c). Stability improvement by covalent attachment of the enzyme then DDM addition, suggests that catalytic current decrease originates from multiple factors, including enzyme leaching and enzyme activity loss.

Temperature is a key factor for the catalytic reaction but also for the stability of the whole system. Chronoamperometry experiments were thus recorded at -0.3V *vs.* Ag/AgCl during consecutive increments of temperatures (Figure SI 3). It can be observed that the enzyme/AuNP biohybrid can work in the full range of temperatures from 30°C to 70°C. A good stability is obtained at 30°C. The current obtained at 70°C is at least four times higher than at the lowest temperature, but it is also less stable mostly because of the instability of the thiol-AuNP architecture at high temperatures. As the temperature decreases back to 60°C, the stability of the system is recovered describing a current more than twice the current recorded at 30°C.

We also carried out hydrogenase immobilization on AuNPs attached to the AuE *via* dithiol bridges (BPDT) (Figure SI 4). Because in this case only an AuNP monolayer was expected to be formed, AuNPs/AuE value was much less yielding values around 1.4. The catalytic process was also very much like the process obtained by immobilization of *Aa* MbH1 on an adsorbed layer of AuNPs directly onto the gold electrode. This confirms that the use of the BPDT as a linker does not preclude electron transfer because of the high conductance of the linker [18]. AuNPs are expected to be strongly attached to the gold surface through the BPDT linker in comparison with AuNPs simply adsorbed. However, the stability of the two bioelectrodes followed by chronoamperometry over 1 h was very similar, suggesting that the attachment of the AuNPs on the gold electrode is not the limiting factor.

The stability of the AuNP/hydrogenase biohybrid was then followed over several days by checking the maximum CV current for H_2 oxidation each day (Figure 5B). The modified electrodes and enzyme solution were daily preserved at 4°C in 10mM phosphate buffer pH 6, previously saturated with N_2 to remove O_2 traces all along the experiments. After 24h the AuNP electrodes keep 20% of the initial current, and after 30 h the current tends to stabilize. During the following days only a slight change is recorded, and the current remains more than 60% of the initial current after 4 days. The AuNP-based bioelectrode appears to be more stable than the previous biohybrid developed in our lab which was based on hydrogenase immobilization in carbon nanofiber network [37] (Figure 5B). This carbon material was proved to be very efficient for direct enzymatic H_2 oxidation leading to current densities higher than 4.5 $mA.cm^{-2}$ (based on the geometric area). However, the CNF/*Aa* MbH1 bioelectrode was shown to be poorly stable with time, losing 50% of current after 48 h, and

90% after 4 days. The absence of covalent attachment between the CNFs and the enzyme can mainly account for this instability. But it is worth noting that the evolution of the catalytic current on CNFs is identical to the evolution of the current recorded with a PG electrode daily freshly modified by the enzyme, and very different from the one recorded at the AuNP modified electrode. This most probably reflects that the AuNP nanostructure is more suitable for enzyme protection than the CNF film.

3.3. H_2/O_2 biofuel cell

AuNP based electrodes were used to build a biofuel cell operating with *Aa* MbH1 at the anode and *Mv* BOD at the cathode (Figure 6). The cell configuration was previously described [6, 8]. The temperature of each half cell, separated by a Nafion membrane, can be independently regulated. The performances of the biocathode and the bioanode were first evaluated in the fuel cell configuration (Figure 6A). To balance the cathodic and anodic sides, AuNPs/AuE values of around 15 and 40 were used for H_2 oxidation and O_2 reduction respectively. A high current density at a temperature of 60°C in the anodic compartment was recorded for H_2 oxidation by hydrogenase, in agreement with the one obtained in the conventional three electrode configuration. Immobilization of *Mv* BOD on AuNP based electrodes was previously studied [22, 30]. Direct electron transfer for O_2 reduction was reported in the case of the commercially available *Mv* BOD on unmodified AuNPs or AuNPs modified by carboxylate-terminated SAMs. Accordingly, we verify in this work that modification of the AuNPs by 3-MPA allows efficient immobilization of *Mv* BOD. Current densities in the order of 0.4 $mA.cm^{-2}$ with an onset around + 0.5 V are obtained for O_2 reduction at a temperature of 25°C and in condition of O_2 bubbling inside the electrolyte of the cathodic compartment (Figure 6A). We noted however that increasing the temperature progressively to 40°C in the cathodic compartment resulted in a progressive decrease of the catalytic activity, as expected for a non thermostable enzyme such as *Mv* BOD.

No covalent attachment was done for the biocathode. Actually, the addition of EDC/NHS resulted in a strong decrease of the catalytic current. Some structural rearrangements were previously suggested in order to explain the decrease in the electron transfer rate after covalent BOD immobilization on gold electrodes [48]. We performed both SDS-PAGE gels and ABTS activity in agarose gels in the presence of *Mv* BOD with increasing EDC/NHS concentrations (i.e. 6/10, 14/21 and 20/30 mM) (data not shown). These gels proved that at least under these experimental conditions no denaturation of the protein occurs. The loss of activity in the present work might imply either structural rearrangement or release of BOD after EDC/NHS treatment on AuNPs modified by MPA. Pita *et al.* also immobilized *Mv* BOD on AuNPs treated through a mixture of MPA and diazonium salts. No deactivation of the enzyme upon covalent attachment was reported, but it was noted that the MPA modification alone resulted in the disappearance of the catalytic signal in serum media [23]. This was attributed to the lower stability of the MPA modification compared to the one prepared by diazonium salt reduction. Accurate assessment is however needed for which coupled spectroscopy/electrochemistry methods would be of great interest.

The open circuit voltage of the biofuel cell was 1.08±0.05 V. Temperature was maintained at 60 °C and 25 °C in the anodic and cathodic compartment respectively. The polarization curve for the biofuel cell is shown in Figure 6B. When decreasing the cell voltage, a sharp increase in the current can be observed at around 0.4 V. The voltage of each electrode was concomitantly monitored during the cell polarization. Because the cathode is the limiting electrode in the system, the BOD bioelectrode varied much more quickly than the hydrogenase bioelectrode. As shown in Figure 6B, the biocathode reaches negative values in the same domain where a sudden increase of the current in the polarization curve is observed.

At these potentials O_2 can be directly reduced at some bare parts of the AuNP electrode, producing hydrogen peroxide. Consequently, whereas the bioanode current was almost unchanged after the polarization experiment, the biocathode lost around 50% in current density (Figure 6A). Attempt to increase the stability of the biocathode by co-immobilization of catalase with *Mv* BOD as proposed in [49] did not result in an improved stability. Nevertheless, at a cell voltage of 0.8 V a power density of 0.25 $mW.cm^{-2}$ is reached (Figure 6C). This power density compares well with the previous power densities reported with the same enzymes immobilized at carbon nanotube networks [8]. In the absence of enzymes, a power density less than 2 $\mu W.cm^{-2}$ is obtained (Figure SI 5). Immobilization of enzymes on AuNPs has been already demonstrated to enhance the power densities of sugars/O_2 EBFC [22]. But this is the first time that a H_2/O_2 biofuel cell based on hydrogenase immobilization on AuNPs is reported. Our results prove that H_2/O_2 biofuel cells can be efficient in many electrode configurations such as carbon nanomaterials but also metal nanoparticles.

4. Conclusion

In this work, the O_2- CO- and temperature-tolerant [NiFe] hydrogenase from *Aquifex aeolicus* hyperthermophilic bacterium was immobilized on gold nanoparticle deposits. For the first time, it is shown that direct H_2 enzymatic oxidation is very efficient on such nanostructured interfaces with no need of any redox mediator and over a large range of temperatures. It is underlined that the microporosity of the AuNP film allows both an enhancement of the electroenzymatic activity beyond the surface enhancement and stabilization with time of the enzyme. Combined with *Mv* BOD at the cathode, a biofuel cell was designed able to deliver a power density of 0.25 $mW.cm^{-2}$. Future work will focus on immobilization of thermostable enzymes on AuNPs for O_2 reduction at high temperatures. This work provides the first investigation of enzymatic H_2 oxidation on nanoparticles which is deisrable to develop coupled methods involving electrochemistry and spectroscopy. This is in progress in the laboratory with the aim to determine the key factors controlling the stability of a bioelectrode as a function of various experimental conditions.

Acknowledgments

The authors thank P. Infossi, Drs M. Guiral, and M.T. Giudici-Orticoni (BIP, Marseille, France) for fruitful discussions, Région Provence-Alpes-Côte d'Azur, Région Aquitaine and ANR for financial support.

References

[1] D. Leech, P. Kavanagh, W. Schuhmann, Enzymatic fuel cells: recent progress, Electrochim. Acta 84 (2012) 223-234.

[2] S. Cosnier, A. Le Goff, M. Holzinger, Toward glucose biofuel cells implanted in human body for powering artificial organs: review, Electrochem. Commun. 38 (2014) 19-23.

[3] D. Pakratov, P. Falkman, Z. Blum, S. Shleev, A hybrid electric power device for simultaneous generation and storage of electric energy, Energ. Environ. Sci. 7 (2014) 989-993

[4] A. de Poulpiquet, D. Ranava, K. Monsalve, MT. Giudici-Orticoni, E. Lojou, Biohydrogen for a new generation of H_2/O_2 biofuel cells: a sustainable energy perspective, ChemElectroChem. 1 (2014) 1724-1750.

[5] L. Xu, F. Armstrong, Optimizing the power of enzyme-based membrane-less hydrogen fuel cells for hydrogen-rich H_2-air mixtures, Energ. Environ. Sci. 6 (2013) 2166-2171.

[6] A. de Poulpiquet, A. Ciaccafava, R. Gadiou, S. Gounel, M.T. Giudici-Orticoni, N. Mano, E. Lojou, Design of a H_2/O_2 biofuel cell based on thermostable enzymes, Electrochem. Com. 42 (2014) 72-74.

[7] S. Krishnan, F. Armstrong, Order-of-magnitude enhancement of an enzymatic hydrogen-air fuel cell based on pyrenyl carbon nanostructures, Chem. Sci. 3 (2012) 1015-1023.

[8] A. Ciaccafava, A. de Poulpiquet, V. Techer, M.T. Giudici-Orticoni, S. Tingry, C. Innocent, E. Lojou, An innovative powerful and mediatorless H_2/O_2 biofuel cell based on an outstanding bioanode, Electrochem. Commun. 23 (2012) 25-28.

[9] M.C. Daniel, D. Astruc, Gold nanoparticles: assembly, supramolecular chemistry, quantum-size-related properties, and applications toward biology, catalysis, and nanotechnology, Chem. Rev. 104 (2004) 293-346.

[10] S. Chen, Y. Liu, Electrochemistry at nanometer-sized electrodes, Phys. Chem. Chem. Phys. 16 (2014) 635-652.

[11] U. Jensen, E. Ferapontova, D. Sutherland, Quantifying protein adsorption and function at nanostructured materials: enzymatic activity of glucose oxidase at GLAD structured electrodes, Langmuir 28 (2012) 11106-11114.

[12] R. Villalonga, P. Diez, P. Yanez-Sedeno, J. Pingarron, Wiring horseradish peroxidase on gold nanoparticles-based nanostructured polymeric network for the construction of mediatorless hydrogen peroxide biosensor, Electrochim. Acta 56 (2011) 4672-4677.

[13] R. Villalonga, P. Diez, M. Eguilaz, P. Martinez, J. Pingarron, Supramolecular immobilization of xanthine oxidase on electropolymerized matrix of functionalized hybrid gold nanoparticles/single-walled carbon nanotubes for the preparation of electrochemical sensors, Appl. Mat. Interfaces 4 (2012) 4312-4319.

[14] T. Meyer, F. Melin, H. Xie, I. von des Hocht, S. Choi, M. Noor, H. Michel, R. Gennis, T. Soulimane, P. Hellwig, Evidence for distinct electron transfer processes in terminal oxidases from different origin by means of protein film voltammetry, J. Am. Chem. Soc. 136 (2014) 10854-10857.

[15] P. Jensen, Q. Chi, F. Grumsen, J. Abad, A. Horsewell, D. Schiffrin, J. Ulstrup, Gold nanoparticles assisted assembly of a heme protein for enhancement of long-range interfacial electron transfer, J. Phys. Chem. C 111 (2007) 6124-6132.

[16] T. Meyer, J. Gross, C. Blanck, M. Schmutz, B. Ludwig, P. Hellwig, F. Melin, Electrochemistry of cytochrome c_1, cytochrome c_{552} and Cu_A from the respiratory chain of *Thermus thermophilus* immobilized on gold nanoparticles, J. Phys. Chem. B 115 (2011) 7165-7170.

[17] F. Melin, T. Meyer, S. Lankiang, S. Choi, R. Gennis, C. Blanck, M. Schmutz, P. Hellwig, Direct electrochemistry of cytochrome *bo3* oxidase at a series of gold nanoparticles-modified electrodes, Electrochem. Commun. 26 (2013) 105-108.

[18] P. Jensen, Q. Chi, J. Zhang, J. Ulstrup, Long-range interfacial electrochemical electron transfer of *Pseudomonas aeruginosa* azurin-gold nanoparticles hybrid systems, J. Phys. Chem. C 113 (2009) 13993-14000.

[19] J. Holland, C. Lau, S. Brozik, P. Atanassov, S. Banta, Engineering of glucose oxidase for direct electron transfer via site-specific gold nanoparticles conjugation, J. Am Chem. Soc. 133 (2011) 19262-19265.

[20] U. Jensen, E. Ferapontova, D. Sutherland, Quantifying protein adsorption and function at nanostructured materials: enzymatic activity of glucose oxidase at GLAD structured electrodes, Langmuir 28 (2012) 11106-11114.

[21] S. Frasca, O. Rojas, J. Salewski, B. Neumann, K. Stiba, I. Weidinger, B. Tiersch, S. Leimkühler, J. Koetz, U. Wollenberger, Human sulfite oxidase electrochemistry on gold nanoparticles modified electrode, Bioelectrochem. 87 (2012) 33-41.

[22] K. Murata, K. Kajiya, N. Nakamura, H. Ohno, Direct electrochemistry of bilirubin oxidase on three-dimensional gold nanoparticles electrodes and its application in a biofuel cell, Energ. Environ. Sci. 2 (2009) 1280-1285.

[23] M. Pita, C. Gutierrez-Sanchez, M. Toscano, S. Shleev, A. de Lacey, Oxygen biosensor based on bilirubin oxidase immobilized on a nanostructured gold electrode, Bioelectrochem. 94 (2013) 69-74.

[24] H. Matsumura, R. Ortiz, R. Ludwig, K. Igarashi, M. Samejima, L. Gorton, Direct electrochemistry of *Phanerochaete chrysosporium* cellobiose dehydrogenase covalently attached on gold nanoparticles modified solid gold electrodes, Langmuir 28 (2012) 10925-10933.

[25] C. Guttierez-Sanchez, M. Pita, C. Vaz-Dominguez, S. Shleev, A. De Lacey, Gold nanoparticles as electronic bridges for laccase-based biocathodes, J. Am. Chem. Soc. 134 (2012) 17212-17220.

[26] C. Lanzellotto, G. Favero, M. Antonelli, C. Tortolini, S. Cannistraro, E. Coppari, F. Mazzei, Nanostructured enzymatic biosensor based on fullerene and gold nanoparticles: preparation, characterization and analytical applications, Biosensors Bioelec. 55 (2014) 430-437.

[27] D. Brondani, N. de Souza, B. Souza, A. Neves, I. Vieira, PEI-coated gold nanoparticles decorated with laccase: a new platform for direct electrochemistry of enzymes and biosensing applications, Biosensors Bioelec. 42 (2013) 242-247.

[28] V. Krikstolaityte, A. Barrantes, A. Ramanavicius, T. Arnebrant, S. Shleev, T. Ruzgas, Bioelectrocatalytic reduction of oxygen at gold nanoparticles modified with laccase, Bioelectrochem. 95 (2014) 1-6.

[29] K. Murata, M. Suzuki, K. Kajiya, N. Nakamura, H. Ohno, High performance bioanode based on direct electron transfer of fructose dehydrogenase at gold nanoparticles-modified electrodes, Electrochem. Commun. 11 (2009) 668-671.

[30] X. Wang, M. Falk, R. Ortiz, H. Matsumura, J. Bobacka, R. Ludwig, M. Bergelin, L. Gorton, S. Shleev, Mediatorless sugar/oxygen enzymatic fuel cells based on gold nanoparticles-modified electrodes, Biosensors Bioelec. 31 (2012) 219-225.

[31] P. Lamberg, S. Shleev, R. Ludwig, T. Arnebrant, T. Ruzgas, Performance of enzymatic fuel cell in cell culture, Biosensors Bioelec. 55 (2014) 168-173.

[32] X. Luo, P. Tron-Infossi, M. Brugna, M.T. Giudici-Orticoni, E. Lojou, Physicochemical key parameters for direct catalytic oxidation of hydrogen by hyperthermophilic [NiFe] hydrogenase immobilized at gold and carbon nanotubes-modified electrodes, J. Biol. Inorg. Chem. 14 (2009) 1275-1288.

[33] M. Pandelia, V. Fourmond, P. Tron-Infossi, E. Lojou, P. Bertrand, C. Leger, MT. Giudici-Orticoni, W. Lubitz, Membrane-bound hydrogenase I from the hyperthermophilic bacterium *Aquifex aeolicus*: enzyme activation, redox intermediates and oxygen tolerance, J. Am. Chem. Soc. 132 (2010) 6991-7004.

[34] E. Lojou, Hydrogenases as catalysts for fuel cells: strategies for efficient immobilization at electrode interfaces, Electrochim. Acta 56 (2011) 10385.

[35] A. De Poulpiquet, A. Ciaccafava, K. Szot, B. Pillain, P. Infossi, M. Guiral, M. Opallo, MT. Giudici-Orticoni, E. Lojou, Exploring properties of a hyperthermophilic membrane-bound hydrogenase at carbon nanotube modified electrodes for a powerful H_2/O_2 biofuel cell, Electroanalysis 25(2013) 685-695.

[36] K. Szot, A. De Poulpiquet, A. Ciaccafava, H. Marques, M. Jonsson-Niedziolka, J. Niedziolka-Jonsson, F. Marken, E. Lojou, M. Opallo, Carbon nanoparticulate films as

effective scaffolds for mediatorless bioelectrocatalytic hydrogen oxidation, Electrochim. Acta 111 (2013) 434-440.

[37] A de Poulpiquet, H. Marques-Knopf, V. Wernert, R. Gadiou, MT. Giudici-Orticoni, E. Lojou, Carbon Nanofiber Mesoporous Films: Efficient Platforms for Bio-Hydrogen Oxidation in Biofuel Cells, Phys. Chem. Chem. Phys. 16 (2014) 1366-1378.

[38] A. Ciaccafava, P. Infossi, M. Ilbert, M. Guiral, S. Lecomte, MT. Giudici-Orticoni, E. Lojou, Electrochemistry, AFM and PM-IRRAS spectroscopy of immobilized hydrogenase: role of a trans-membrane helix on enzyme orientation for efficient H_2 oxidation, Angew. Chem. Int. Ed. 51(2012)953-956.

[39] A. Ciaccafava, A. De Poulpiquet, P. Infossi, S. Robert, R. Gadiou, M.T. Giudici-Orticoni, S. Lecomte, E. Lojou, A friendly detergent for H_2 oxidation by *Aquifex aeolicus* membrane-bound hydrogenase immobilized on graphite and SAM-modified gold electrodes, Electrochim. Acta 82 (2012) 115-125.

[40] F. Oteri, A. Ciaccafava, A. de Poulpiquet, E. Lojou, M. Baaden, S. Sacquin-Mora, Fluctuations in the dipole moment of membrane-bound hydrogenase from *Aquifex aeolicus* account for its adaptability to charged electrodes, Phys. Chem. Chem. Phys. 16 (2014) 11318-11322.

[41] S. Trasatti, O. Petrii, Real surface area measurements in electrochemistry, Pure Appl. Chem. 63 (1991) 711-734.

[42] G. Frens, Controlled Nucleation for the Regulation of the Particle Size in Monodisperse Gold Suspensions, Nature Phys. Sci. 241 (1973) 20-22.

[43] W. Haiss, N. Thanh, J. Aveyard, D. Fernig, Determination of size and concentration of gold nanoparticles from UV-Vis spectra, Anal. Chem. 79 (2007) 4215-4221.

[44] S. Link, M. A. El-Sayed, Size and temperature dependence of the Plasmon absorption of colloidal gold nanoparticles, J. Phys. Chem. B 103 (1999) 4212-4217.

[45] K. Murata, K. Kajiya, Y. Suga, T. Watanabe, N. Nakamura, H. Ohno, A simple fabrication method for three-dimensional gold nanoparticles electrodes and their application to the study of the direct electrochemistry of cytochrome c, Electroanalysis 22 (2010) 185-190.

[46] O. Rüdiger, C. Gutiérrez-Sánchez, D. Olea, I. Pereira, M. Vélez, V.M. Fernández, A.L. De Lacey, Enzymatic Anodes for Hydrogen Fuel Cells based on Covalent Attachment of Ni-Fe Hydrogenases and Direct Electron Transfer to SAM-Modified Gold Electrodes, Electroanalysis, 22 (2010) 776-783.

[47] D. Pankratov, R. Sundberg, D. B. Suyatin, J. Sotres, A. Barrantes, T. Ruzgas, I. Maximov, L. Montelius, S. Shleev, The influence of nanoparticles on enzymatic bioelectrocatalysis, RSC Adv. 4 (2014) 38164-38168.

[48] K. Singh, T. McArdle, P. Sullivan, C. Blanford, Sources of activity loss in the fuel cell enzyme bilirubin oxidase, Energ. Environ. Sci. 6 (2013) 2460-2464.

[49] S. Shleev, G. Shumakovich, O. Morozova, A. Yaropolov, Stable 'Floating' Air Diffusion Biocathode Based on Direct Electron Transfer Reactions Between Carbon Particles and High Redox Potential Laccase, Fuel Cells, 10 (2010) 726-733.

Legends

Figure 1: Size distribution and morphology of the gold nanoparticles. (A) AuNP hydrodynamic size distribution by DLS; (B) UV-visible spectra of AuNPs obtained with 38.8 mM (bold line), and 19.4 mM (dot-dashed line) sodium citrate; TEM images of AuNPs synthesized with 38.8 mM (C) and 19.4 mM (D) sodium citrate.

Figure 2: (A) CVs of gold electrodes modified with consecutive AuNP drop castings: 1 (grey line), 3 (dashed line), 4 (dotted line) deposits; Inset: CV of the bare polycrystalline gold electrode; (B) AuNPs/AuE values as a function of AuNP casting number. 0.05 M H_2SO_4; scan rate 0.1V/s under N_2 atmosphere and room temperature. (C) SEM image of the top view of the AuNP modified gold surface.

Figure 3: CVs for H_2 oxidation by *Aa* MbH1 immobilized on a gold electrode modified with one AuNP deposit: (a) H_2 in over pressure above the electrolyte; (b) H_2 in continuous flow in the electrolyte solution; (c) H_2 is replaced by N_2. 10 mM phosphate buffer, pH 6, 60°C, 5 mV/s.

Figure 4: (A) H_2 catalytic currents for increasing AuNPs/AuE values (a) 28, (b) 38 and (c) 50. Inset: H_2 oxidation by *Aa* MbH1 absorbed on a bare gold electrode (B) Catalytic current densities for H_2 oxidation reported to the electroactive surface area of the AuNP deposit as a function of AuNPs/AuE. 10 mM phosphate buffer, pH 6, 60°C under H_2 flow, 5mV/s.

Figure 5: (A) H_2 oxidation current loss with the *Aa* MbH1 immobilized on 4-ATP modified AuNPs: (a) without EDC/NHS (dotted line), (b) with EDC/NHS (dashed line); (c) with EDC/NHS and 3CMC DDM addition (solid line). E = -0.3 V *vs.* Ag/AgCl, 10 mM phosphate buffer, pH 6, 60°C under H_2 flow; (B) long term H_2 oxidation current loss with the *Aa* MbH1 immobilized on (a) CNF modified PG electrode (dotted line), (b) freshly daily adsorbed on bare PG electrode (dashed line), (c) covalently bounded to 4-ATP modified AuNP gold electrode (solid line); 60°C under H_2 flow, 5 mV/s.

Figure 6: (A) Direct H_2 oxidation and O_2 reduction at AuNP nanostructured electrodes in the fuel cell configuration, before (solid line) and after (dashed line) cell measurements; (B) Polarization curve of AuNP-based H_2/O_2 biofuel cell (black line) and cathode potential evolution during the polarization experiment (grey line); (C) Operational performance of the AuNP-based H_2/O_2 biofuel cell: power density (grey line) and cell voltage (black line) as a function of the current density. 10mM phosphate buffer pH 7, under continuous H_2 (bioanode) or O_2 (biocathode) flow, 3 mV/s.

Supplemental Informations

Surface Increment	I_{pa} / A	I_{pc} / A	Γ / mol.cm^{-2}	E_m / V	△E	Γ Increment
1	$3.5\ 10^{-9}$	$5.7\ 10^{-9}$	$7.6\ 10^{-12}$	0.004	0.027	1
20	$7.9\ 10^{-8}$	$7.8\ 10^{-8}$	$1.3\ 10^{-10}$	0.009	0.002	17.7
36	$2.3\ 10^{-7}$	$2.4\ 10^{-7}$	$3.9\ 10^{-10}$	0.001	0.002	51.5

Table 1: Electrochemistry of Horse heart cytochrome c at 6-MHA-AuNP modified gold electrode. I_{pa} and I_{pc}: anodic and cathodic peak currents respectively, Γ: protein surface coverage, E_m : average redox potential, ΔE : potential difference between the anodic and cathodic peak potentials. 10 mM phosphate buffer pH 6, 0.1V/s.

Figure SI 1: CVs for H_2 oxidation on AuNP deposit in the absence of *Aa* MbH1; 10 mM phosphate buffer pH 6, 60°C under continuous H_2 flow, 5 mV/s.

Figure SI 2: Comparative CVs for H_2 oxidation by *Aa* MbH1 covalently immobilized on (a) 25 nm AuNPs and AuNPs/AuE of 14 (solid line) and (b) 35 nm AuNPs and AuNPs/AuE of 3 (dashed line). 10 mM phosphate buffer pH 6, 60°C under continuous H_2 flow, 5 mV/s.

Figure SI 3: Chronoamperometry measurement at -0.3V *vs.* Ag/AgCl for H_2 oxidation current at consecutive temperature increasing conditions. 10 mM phosphate buffer pH 6, 60°C under continuous H_2 flow.

Figure SI 4: CVs for H_2 oxidation by *Aa* MbH1 covalently immobilized on a gold electrode modified with AuNPs on a BPDT layer (dashed line), or AuNPs directly adsorbed on the gold electrode (solid line). 10 mM phosphate buffer pH 6, 60°C under continuous H_2 flow, 5 mV/s.

Figure SI 5: Polarization and power curves on AuNPs in the absence of enzymes. 10mM phosphate buffer pH 7, under continuous H_2 (bioanode) or O_2 (biocathode) flow, 3 mV/s.

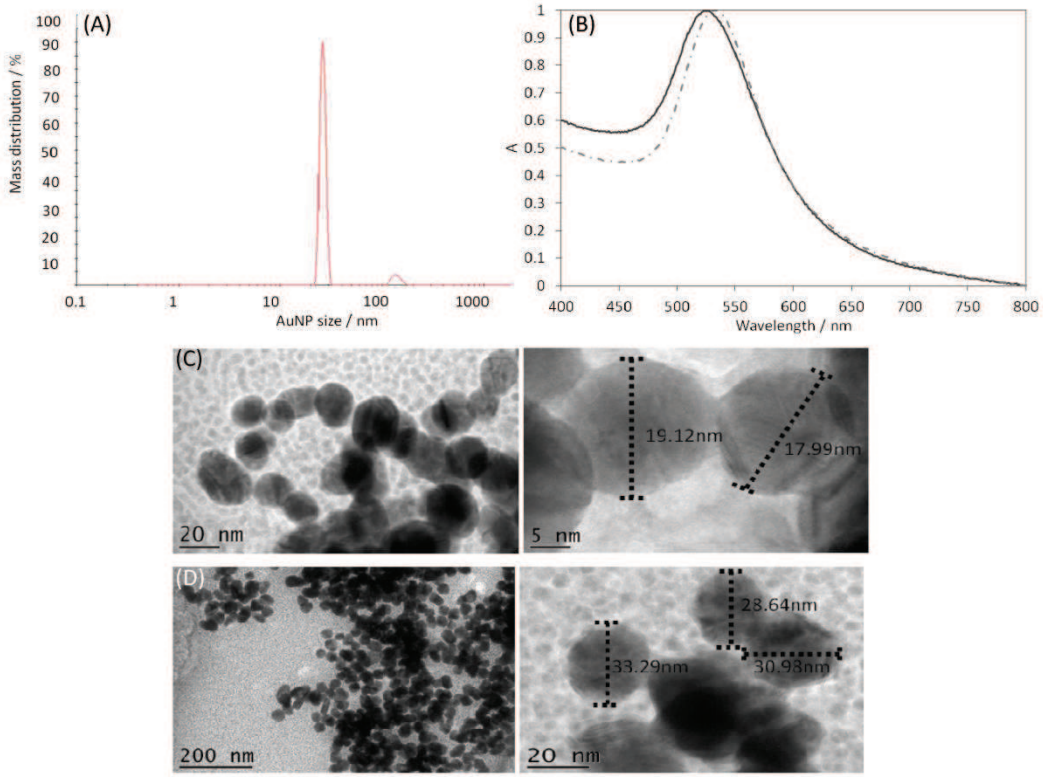

Fig. 1

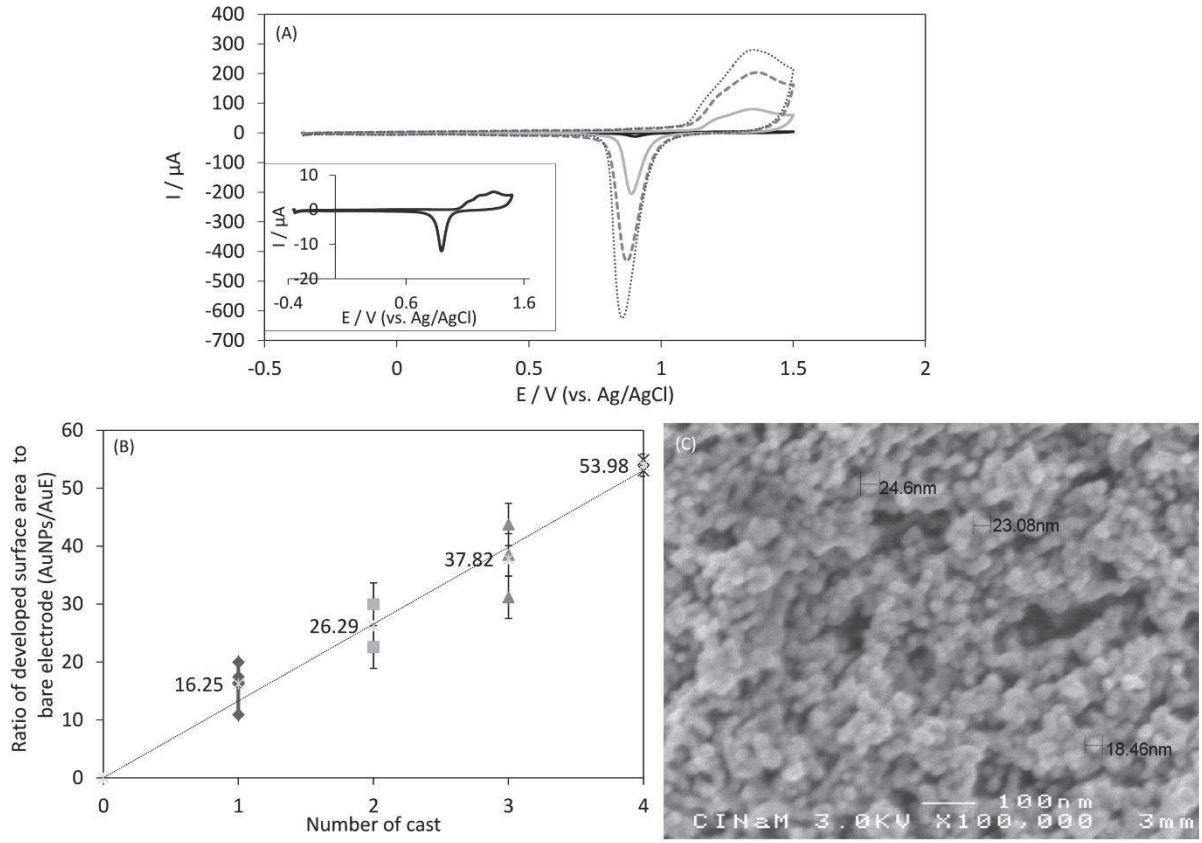

Fig. 2

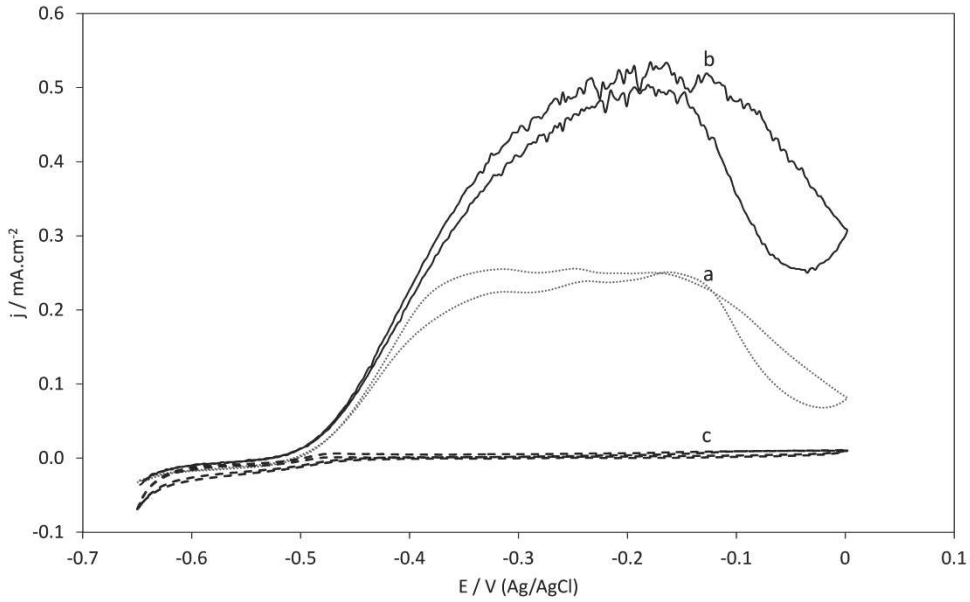

Fig. 3

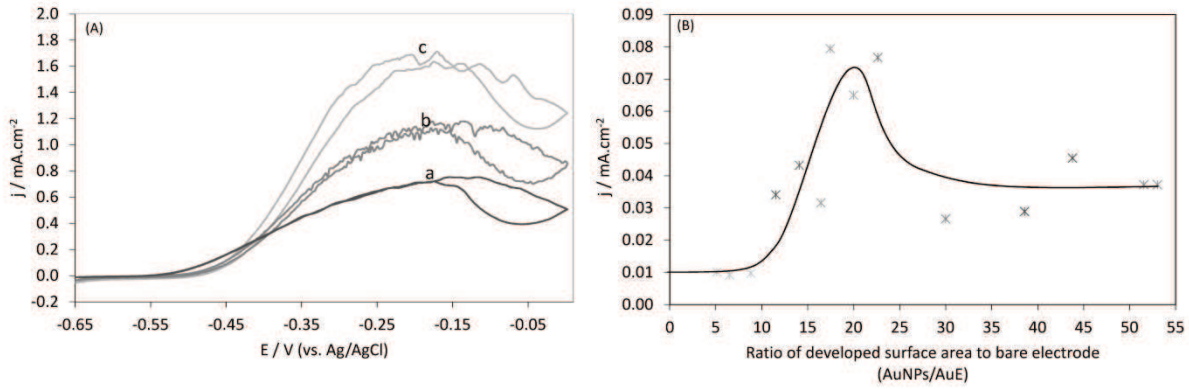

Fig. 4

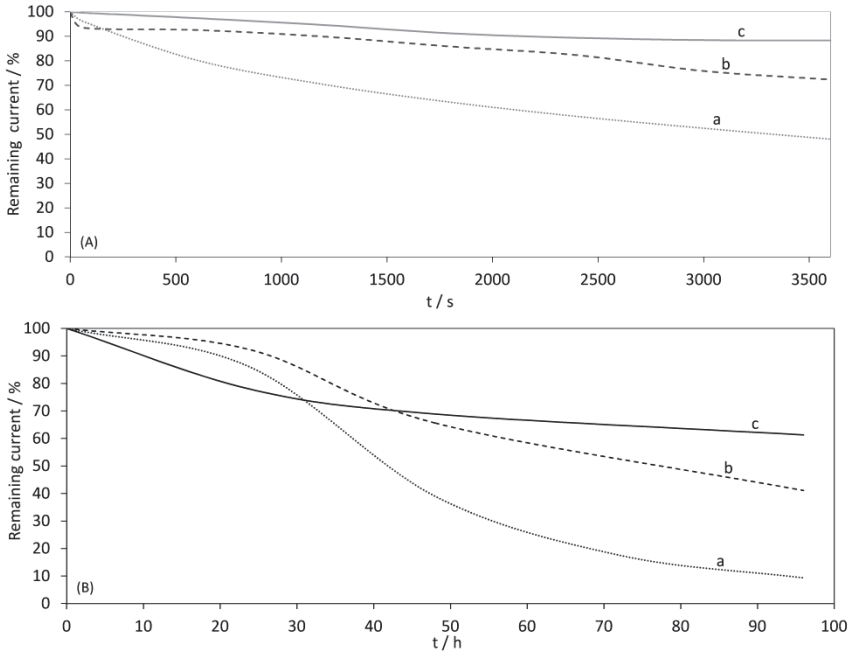

Fig. 5

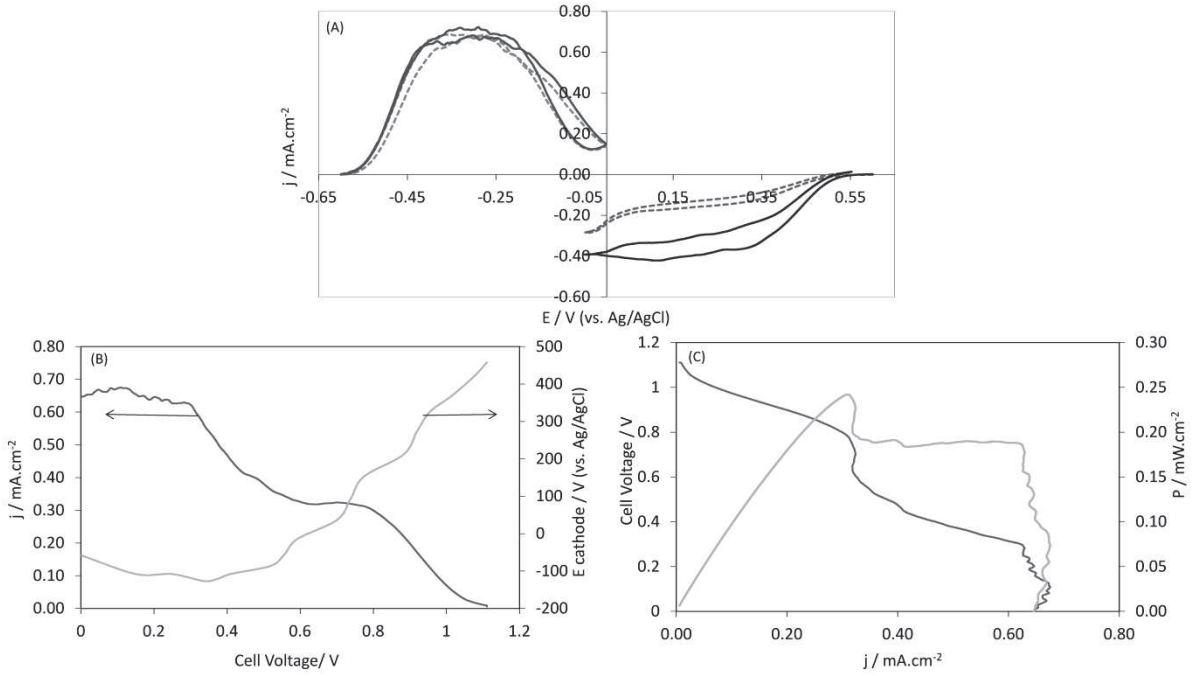

Fig. 6

Highlights

- 20.0±5.3 and 37.2±4.3 nm gold nanoparticles were deposited on a gold electrode
- O_2- and CO-tolerant [NiFe] hydrogenase was immobilized on the AuNP deposits
- Direct H_2 oxidation was obtained with current densities up to 1.85±0.15 $mA.cm^{-2}$
- A biofuel cell was designed delivering 0.25 $mW.cm^{-2}$